Supplementary Appendix

Data Sources

This study was granted an exemption by our Institutional Review Board in April 2023, classifying the project as Secondary Research (research involving only information collection and analysis involving the investigator's use of identifiable health information when that use is for the purposes of research). Data about the patient's case and clinical care were abstracted from the patient's electronic medical record (EMR) at St. Jude Children's Research Hospital (SJCRH). Photographs of bone marrow histology were taken by a pathologist.

The germline *BARD1* and somatic mutations were reported as part of the St. Jude Clinical Genomics (ClinGen) program which employs three-platform whole-genome (WGS), whole-exome (WES) and transcriptome (RNA-Seq) sequencing to report somatic and germline pathogenic/likely pathogenic variants[1]. A modified version of a two-platform (WES and RNA-Seq) pipeline was later developed for analyzing FFPE samples, which included our index patient sample (ID SJNBL031647). ClinGen genomic data from consented patients are uploaded to St. Jude Cloud[2], where we obtained the BAM files (WES and RNA-Seq) used in this study. In addition to the index patient, fifty-eight (58) other neuroblastomas profiled by ClinGen during 2016–2019 were included in the synthetic lethality score estimation (Table S1).

The pathogenic germline *BARD1* mutation identified in our index patient is a 2-bp deletion located at chr2: 215,646,058–215,646,059 in GRCh37 coordinates. It causes a frameshift mutation in exon 4 of *BARD1* (NM_000465.4:c.539_540del, p. S179_Y180fs), which matches a known pathogenic ClinVar variant (VCV000186576) previously found in families with breast and ovarian cancer.

Analysis of Bi-allelic Loss of *BARD1*

To assess the allelic state of the 2-bp germline mutation *BARD1* S179_Y180fs at chr2: 215,646,058–215,646,059 in GRCh37 coordinates (Fig. S1B) in the tumor genome of the index patient, we first obtained the unique read counts of wildtype and mutant alleles in WES and RNA-Seq BAM files by running indelPost[3], a software tool that performs indel re-alignment to ensure accuracy. This resulted in a VAF of 0.5, 0.4 and 0.8 in germline DNA, tumor DNA and tumor RNA, respectively, indicating absence of LOH in tumor but a possible second hit causing allelic-specific expression (ASE). To further investigate ASE, we incorporated 4 germline heterozygous SNPs at the *BARD1* locus (chr2: 215590370-215674407) with ≥5 RNA-Seq reads. These SNPs (i.e., rs2070096 [gNOMAD WGS (https://gnomad.broadinstitute.org/) population frequency for the non-reference allele: 0.2], rs2229571 [0.53], rs2070094 [0.35], and rs5020511 [0.65]) were identified by GATK HaplotypeCaller (ver. 4.0.2.1)[4] analysis of WES BAM files. The lack of a second hit in DNA has also been verified by exome CNV analysis[5]. By contrast, ASE was detected across all 4 SNPs along with the mutation site in tumor RNA-seq (main Fig. 1b). The varying population frequencies project the existence of multiple haplotypes with different allelic combinations. The human reference genome used for RNA-Seq mapping represents a haplotype consisting of major, minor, major, and minor alleles of the four SNPs. The ASE in patient RNA-Seq indicates the existence of a haplotype comprised of minor, minor, minor, and major alleles of the four SNPs. This pattern explains the retained reference allele of SNP2 (which is the minor allele of the general population) in contrast to the non-reference alleles in the other three SNPs in the index patient RNA-Seq data.

We used a binomial distribution model to evaluate the significance of ASE in S179_Y180fs and the four SNPs assuming a DNA VAF of 0.5, which was modelled by binomial distribution:

$$\sum_{SNPs} |binom(cov, p)/cov - 0.5|, \ \ where\ cov\ is\ RNA\ coverage\ for\ each\ SNP\ and\ p = 0.5.$$

The observed RNA VAF deviation of the five variants was similarly calculated as follows.

$$\sum_{SNPs} |RNA\ VAF_{observed} - 0.5| = 1.264$$

We then performed a simulation by running the binomial model 1,000 times and found only VAF deviation >1.264 occurred 15 times, which gives a significant *p*-value of 0.015 for the observed ASE. Histology-based VAF adjustment with tumor purity supported the monoallelic expression of the mutant allele tumor, which was performed as:

$$VAF_{adjusted} = \ \{VAF_{observed} - 0.5 \cdot (1 - purity)\}/purity$$

Immunohistochemical Staining

Immunohistochemical staining (IHC) was performed using the Leica BOND RX Autostainer (Leica Biosystems, Deer Park, Illinois, USA) in the Anatomic Pathology/Neuropathology Translation Support lab in the Department of Pathology at St. Jude Children's Research Hospital. FFPE sections were heated for one hour at 68ºC prior to placement on the instrument. The BOND Polymer Refine IHC Protocol F was selected. Heat induced epitope retrieval, ER1, was used for 20 minutes. 150 uL 1:20 dilution of BARD1 (E-11) (Santa Cruz Biotechnology, Inc, Dallas, Texas, USA) was applied with an incubation of 15 minutes for detection. All slides were counterstained with hematoxylin for 5 minutes. Tumor cells, which resemble differentiating

ganglion cells, were identified by morphologic assessment by board-certified pediatric pathologists (i.e. co-authors S.C.K. and B.A.O.)

Synthetic Lethality Score

The PARPi prediction pipeline[6] was adapted from previously published SELECT[7] and ENLIGHT[8] pipelines to predict drug response in pediatric populations based on the identification of three types of genetic interaction partners of *PARP1* and *PARP2*, the primary targets of talazoparib. Those include synthetic lethal (SL), synthetic dosage lethal (SDL) and synthetic rescue (SR) partner genes. The pipeline begins with selecting all genes phylogenetically similar to the given *PARP* genes from > 20,000 protein coding genes. Subsequent steps prioritize the genetic partners further, analyzing the transcriptome and survival datasets from two pediatric cancer cohorts: the INdividualized therapy FOr Relapsed Malignancies in childhood (INFORM) consortium (n = 519)[9] and the Therapeutically Applicable Research to Generate Effective Treatments (TARGET) consortium (n = 614). In brief, in these steps, the genetic partners are further refined to include only those that occur less frequently than a random chance by hypergeometric test, reflecting the notion that cancer cells where such pairs of genes are functionally interacting (e.g., both inactive in the case of synthetic lethal partners) would be selected against. For such pairs of genetically interacting genes, Cox-proportional hazard modelling was performed to further identify interactions that offer a survival advantage (thus reflecting the notion that they indeed decrease tumor fitness). This process results in identifying two sets of genetic interaction partners, one for *PARP1* and one for *PARP2.* These sets then serve to create a synthetic lethality score on a zero-to-one scale for each tumor sample based on the activity state of the partner genes, as inferred from the tumor transcriptome.

Supplementary Figure S1.

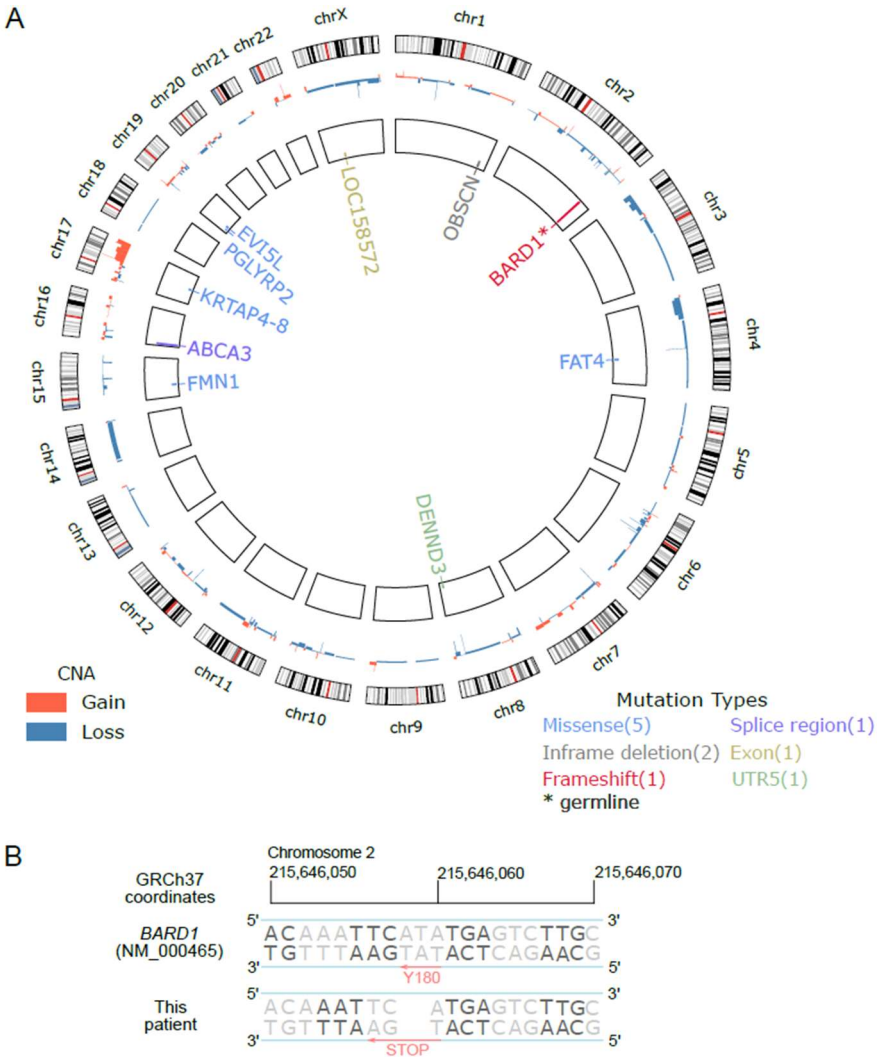

Genomic landscape of the index patient. **A.** Along the chromosomes (*outer track*), copy-number alterations (CNA) (*middle track*) and short mutations (*inter track*) are plotted as identified by tumor/normal-paired whole-exome sequencing. This index patient had segmental chromosome losses (3p and 4p) and gains (11q13.3 and 17q), which are recurrent in neuroblastoma. There was no *MYCN* amplification nor 11q loss at the *ATM* locus. Additionally, somatic and P/LP germline mutations were absent at the *ATM* locus. Somatic short mutations were also shown with variant allele frequency (bar plots along gene). The highest frequency was 0.35 for *ABCA3*, which is in good agreement with the histological tumor purity assessment of 60%. These ten somatic mutations (2 mutations in *OBSCN*) are not known drivers in neuroblastoma. **B.** Illustration of the *BARD1* germline frameshift in the 20-bp genomic region (chr2: 215,646,050–215,646,070 on GRCh37). The transcript NM_000465 is used to show the amino acid change. In this patient, the 2-bp deletion removes the adenine(A) and thymine (T) bases in codon Y180 resulting in an immediate stop codon. At the *BARD1* locus, there is no second hit in tumor DNA given the absence of copy-number alterations, loss-of-heterozygosity, or additional germline/somatic mutations. This suggests that epigenetic silencing is a potential mechanism for the allele-specific expression of frameshift mutation. Other deleterious germline mutations were not found in homologous recombination deficiency-related genes.

Supplementary Figure S2.

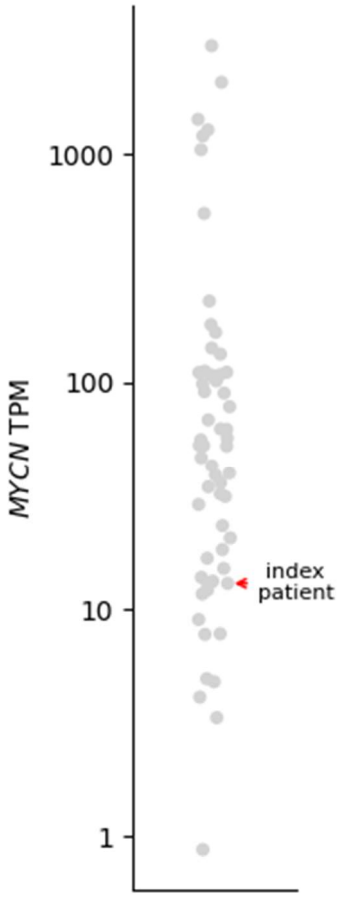

***MYCN* expression levels of the 59 neuroblastomas profiled by St. Jude clinical genomic sequencing program during 2016-2019.** The neuroblastoma of the index patient is indicated by a red arrow. *MYCN* expression level, plotted as transcript per million (TPM), was previously reported to be associated with increased replication stress and sensitivity to PARPi in neuroblastoma cell line models[10].

Supplementary Figure S3.

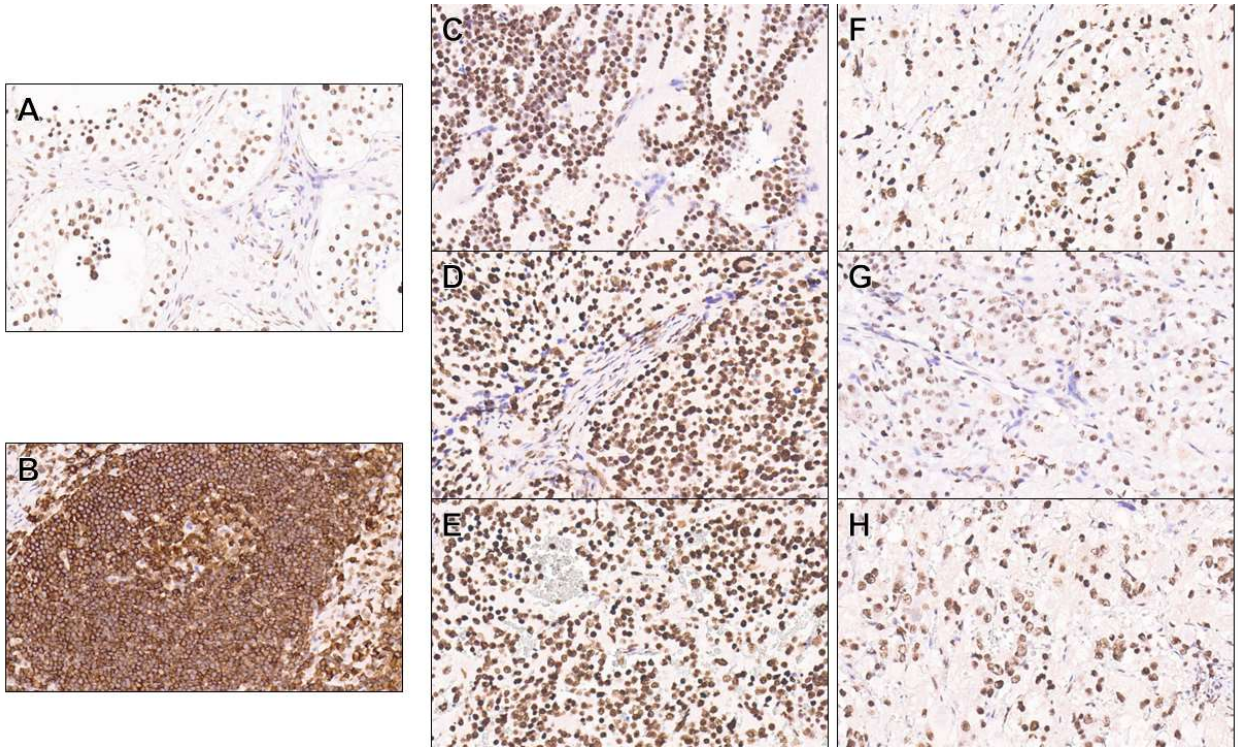

Control BARD1 staining in normal tissues and other neuroblastomas. A) testis. B) lymph node. C–E) pre-treatment neuroblastomas. F–H) post-treatment. In this control experiment. BARD1 protein was diffusely expressed in all twenty neuroblastomas with no known *BARD1* variants. Six separate representative cases are shown in images C–H.

Supplementary Table 1.

Sample_name	Accession_ID	PARP1 SLscore	PARP2 SLscore	PARP1 TPM	PARP2 TPM
SJNBL030096_D1	SJC-DS-1004	0.3	0.21	233.1836573	23.77278777
SJNBL030107_D1	SJC-DS-1004	0.48	0.21	122.1781086	41.1405367
SJNBL030147_D1	SJC-DS-1004	0.35	0.42	101.7738697	39.64633341
SJNBL030152_D1	SJC-DS-1004	0.45	0.37	164.8842179	31.22788356
SJNBL030158_D1	SJC-DS-1004	0.57	0.26	152.0182999	65.15960651
SJNBL030177_D1	SJC-DS-1004	0.43	0.26	199.1792982	70.79588765
SJNBL030203_D1	SJC-DS-1004	0.22	0.32	62.31342128	31.20580859
SJNBL030224_D1	SJC-DS-1004	0.43	0.26	139.9735696	46.42007721
SJNBL030259_D1	SJC-DS-1004	0.3	0.21	145.4419801	41.68143779
SJNBL030307_D1	SJC-DS-1004	0.52	0.58	149.6317898	37.755601
SJNBL030309_D1	SJC-DS-1004	0.36	0.32	140.5489726	46.93805971
SJNBL030339_D1	SJC-DS-1004	0.38	0.68	96.42875017	37.27187703
SJNBL030342_D1	SJC-DS-1007	0.16	0	80.4890933	21.69289413
SJNBL030412_D1	SJC-DS-1007	0.44	0.74	126.8634007	97.85585008
SJNBL030452_D1	SJC-DS-1007	0.4	0.63	143.5417499	37.05283415
SJNBL030513_D1	SJC-DS-1007	0.46	0.53	105.653593	32.75333563
SJNBL030513_D2	SJC-DS-1007	0.22	0.32	81.86154816	27.31251121
SJNBL030555_D1	SJC-DS-1007	0.43	0.11	280.8878444	31.34640734
SJNBL030623_D1	SJC-DS-1007	0.5	0.79	126.756016	45.59488749
SJNBL030641_D1	SJC-DS-1007	0.31	0.32	207.1638979	41.14873954
SJNBL030694_D1	SJC-DS-1007	0.48	0.58	137.1515298	70.44287047
SJNBL030721_D1	SJC-DS-1007	0.29	0	54.79336148	6.668919256
SJNBL030749_D1	SJC-DS-1007	0.16	0.16	91.76343381	17.65829868
SJNBL030758_D1	SJC-DS-1007	0.27	0.42	119.0720945	17.38479825
SJNBL030793_D1	SJC-DS-1007	0.57	0.37	112.7420875	22.61276694
SJNBL030793_D2	SJC-DS-1007	0.3	0.42	93.12528406	21.29980114
SJNBL030810_D1	SJC-DS-1007	0.33	0	63.47596232	31.44466973
SJNBL030810_D2	SJC-DS-1007	0.19	0.32	68.95845554	23.72555844
SJNBL030820_D1	SJC-DS-1007	0.37	0.37	135.0020327	36.07917189
SJNBL030824_D1	SJC-DS-1007	0.54	0.58	202.3067511	24.26566686
SJNBL030842_D1	SJC-DS-1007	0.26	0.11	37.98724479	18.90605652
SJNBL030875_D1	SJC-DS-1007	0.21	0.37	108.1843015	30.68664561
SJNBL030882_D1	SJC-DS-1007	0.36	0.42	121.8328436	23.05116498
SJNBL030917_D1	SJC-DS-1007	0.1	0.16	69.71415437	12.94898744
SJNBL030925_D1	SJC-DS-1007	0.09	0.11	55.44528111	17.67373534
SJNBL030925_D2	SJC-DS-1007	0.34	0.63	94.99877614	44.86933486
SJNBL030939_D1	SJC-DS-1007	0.18	0.26	107.990973	30.07915036
SJNBL030955_D1	SJC-DS-1007	0.2	0.58	89.31954843	21.14450286
SJNBL030995_D1	SJC-DS-1007	0.34	0.21	85.20199645	15.46453976
SJNBL031046_D2	SJC-DS-1007	0.23	0.26	89.98636315	18.92320605
SJNBL031046_D3	SJC-DS-1007	0.36	0.26	174.2151551	37.9476927
SJNBL031053_D1	SJC-DS-1007	0.46	0.42	124.3634155	40.05044107
SJNBL031070_D1	SJC-DS-1007	0.24	0.32	111.2539935	20.29404496
SJNBL031145_D1	SJC-DS-1007	0.33	0.53	74.84102568	29.24807902
SJNBL031159_D2	SJC-DS-1007	0.15	0	65.6113555	13.69252567
SJNBL031159_D3	SJC-DS-1007	0.2	0.26	62.33621693	19.43688514
SJNBL031228_D1	SJC-DS-1007	0.16	0.05	76.23088794	13.25079077
SJNBL031232_D1	SJC-DS-1007	0.23	0.26	74.86050536	26.06356635
SJNBL031239_D1	SJC-DS-1007	0.48	0.16	170.29715	32.76057733
SJNBL031246_D1	SJC-DS-1007	0.25	0.32	87.94461051	16.81549931
SJNBL031261_D1	SJC-DS-1007	0.25	0.42	79.60864964	32.18767881
SJNBL031277_D1	SJC-DS-1007	0.38	0.21	157.2678658	28.39156342
SJNBL031338_D1	SJC-DS-1007	0.39	0.32	192.0068632	34.35725902
SJNBL031497_D1	SJC-DS-1007	0.23	0.32	102.9502992	31.35949758
SJNBL031559_D1	SJC-DS-1007	0.52	0.68	140.0300909	54.12025623
SJNBL031585_D1	SJC-DS-1007	0.32	0.42	145.8651657	18.20733535
SJNBL031598_D1	SJC-DS-1007	0.41	0.32	126.1920919	50.82745144
SJNBL031647_D1	**SJC-DS-1007**	**0.34**	**0.84**	**64.14168736**	**39.61718932**
SJNBL031668_D1	SJC-DS-1007	0.29	0.05	36.83239218	15.25959351

Synthetic lethality scores in neuroblastoma cohort. Synthetic lethality scores (SL core) against *PARP1/2* inhibition are shown for the index sample (SJNBL031647_D1 in bold) and other 58 neuroblastoma patient samples profiled by St. Jude clinical sequencing program during 2016-2019. Accession ID: dataset accession to the sequencing data on St. Jude Cloud. TPM: transcript per million

References

1. Rusch M, Nakitandwe J, Shurtleff S, et al. Clinical cancer genomic profiling by three-platform sequencing of whole genome, whole exome and transcriptome. Nat Commun. 2018 Sep 27;9(1):3962. doi: 10.1038/s41467-018-06485-7.

2. McLeod C, Gout AM, Zhou X, et al. St. Jude Cloud: A Pediatric Cancer Genomic Data-Sharing Ecosystem. Cancer Discov 2021;11(5):1082-1099. (In eng). DOI: 10.1158/2159-8290.Cd-20-1230.

3. Hagiwara K, Edmonson MN, Wheeler DA, Zhang J. indelPost: harmonizing ambiguities in simple and complex indel alignments. Bioinformatics 2022;38(2):549-551. (In eng). DOI: 10.1093/bioinformatics/btab601.

4. DePristo MA, Banks E, Poplin R, et al. A framework for variation discovery and genotyping using next-generation DNA sequencing data. Nat Genet 2011;43(5):491-8. (In eng). DOI: 10.1038/ng.806.

5. Talevich E, Shain AH, Botton T, et al. CNVkit: Genome-Wide Copy Number Detection and Visualization from Targeted DNA Sequencing. PLoS Comput Biol. 2016 Apr 21;12(4):e1004873. doi: 10.1371/journal.pcbi.1004873.

6. Nagy M, Schischlik F, Wang K, et al. Abstract 3118: Predicting response to PARP inhibitors in pediatric cancer via synthetic lethal networks. Cancer Research 2023;83(7_Supplement):3118-3118. DOI: 10.1158/1538-7445.Am2023-3118.

7. Lee JS, Nair NU, Dinstag G, et al. Synthetic lethality-mediated precision oncology via the tumor transcriptome. Cell 2021;184(9):2487-2502.e13. (In eng). DOI: 10.1016/j.cell.2021.03.030.

8. Dinstag G, Shulman ED, Elis E, et al. Clinically oriented prediction of patient response to targeted and immunotherapies from the tumor transcriptome. Med 2023;4(1):15-30.e8. (In eng). DOI: 10.1016/j.medj.2022.11.001.

9. van Tilburg CM, Pfaff E, Pajtler KW, et al. The Pediatric Precision Oncology INFORM Registry: Clinical Outcome and Benefit for Patients with Very High-Evidence Targets. Cancer Discovery 2021;11(11):2764-2779. DOI: 10.1158/2159-8290.Cd-21-0094.

10. King D, Li XD, Almeida GS, et al. MYCN expression induces replication stress and sensitivity to PARP inhibition in neuroblastoma. Oncotarget. 2020;11(23):2141-2159.

Author contributions

S.F. developed the treatment of the patient. K.H. performed the genomic analysis and discovered the bi-allelic loss of *BARD1*. M.C., K.H., J.Z. and S.F. prepared the first draft of the manuscript. M.N. and E.R. analyzed the synthetic lethality score. S.C.K., B.A.O, and J.E. performed immunohistochemistry staining and histological annotation. J.Z. designed the genomic analysis, planned result validation, and supervised the analysis. All authors contributed to the writing and revision of the manuscript.

Acknowledgments

This work was supported in part by National Cancer Institute (NCI) grant R01CA216391 to JZ and a Cancer Center Support (CORE) Grant (P30 CA21765) to St. Jude Children's Research Hospital. All authors received support from American Lebanese Syrian Associated Charities (ALSAC). We thank the St Jude Clinical Genomics program for generating the genomic data used in this study. We also thank Mahsa Khanlari, MD, for providing photographs of the patient's bone marrow histology and Heather Mulder for helping with sample processing. We thank the Anatomic Pathology/Neuropathology Translation Support lab in the Department of Pathology at St. Jude Children's Research Hospital for developing and performing the BARD1 immunohistochemical staining protocol. We would like to appreciate Mr. Michael N. Edmonson for proofreading the manuscript.